materials

MDPI

Article

Magnetic Biochar Obtained by Chemical Coprecipitation and Pyrolysis of Corn Cob Residues: Characterization and Methylene Blue Adsorption

Norma Araceli Guel-Nájar [1], Jorge Carlos Rios-Hurtado [1,*], Elia Martha Muzquiz-Ramos [2], Gloria I. Dávila-Pulido [3], Adrián A. González-Ibarra [3] and Aurora M. Pat-Espadas [4]

[1] Facultad de Metalurgia, Universidad Autónoma de Coahuila, Carretera 57 Km 5, Monclova 25710, Coahuila, Mexico; normaguel@uadec.edu.mx
[2] Facultad de Ciencias Químicas, Universidad Autónoma de Coahuila, Blvd. Venustiano Carranza S/N, República, Saltillo 25280, Coahuila, Mexico
[3] Escuela Superior de Ingeniería, Universidad Autónoma de Coahuila, Boulevard Adolfo López Mateos S/N, Independencia, Nueva Rosita 26830, Coahuila, Mexico; gloriadavila@uadec.edu.mx (G.I.D.-P.); gonzalez-adrian@uadec.edu.mx (A.A.G.-I.)
[4] CONACyT, Estación Regional del Noroeste del Instituto de Geología de la UNAM, Luis D Colosio S/N Esquina Madrid, Hermosillo 83200, Sonora, Mexico; apespadas@geologia.unam.mx
* Correspondence: jorgerios@uadec.edu.mx

Abstract: Biochar is a carbonaceous and porous material with limited adsorption capacity, which increases by modifying its surface. Many of the biochars modified with magnetic nanoparticles reported previously were obtained in two steps: first, the biomass was pyrolyzed, and then the modification was performed. In this research, a biochar with Fe_3O_4 particles was obtained during the pyrolysis process. Corn cob residues were used to obtain the biochar (i.e., BCM) and the magnetic one (i.e., BCM_{Fe}). The BCM_{Fe} biochar was synthesized by a chemical coprecipitation technique prior to the pyrolysis process. The biochars obtained were characterized to determine their physicochemical, surface, and structural properties. The characterization revealed a porous surface with a 1013.52 m^2/g area for BCM and 903.67 m^2/g for BCM_{Fe}. The pores were uniformly distributed, as observed in SEM images. BCM_{Fe} showed Fe_3O_4 particles on the surface with a spherical shape and a uniform distribution. According to FTIR analysis, the functional groups formed on the surface were aliphatic and carbonyl functional groups. Ash content in the biochar was 4.0% in BCM and 8.0% in BCM_{Fe}; the difference corresponded to the presence of inorganic elements. The TGA showed that BCM lost 93.8 wt% while BCM_{Fe} was more thermally stable due to the inorganic species on the biochar surface, with a weight loss of 78.6%. Both biochars were tested as adsorbent materials for methylene blue. BCM and BCM_{Fe} obtained a maximum adsorption capacity (q_m) of 23.17 mg/g and 39.66 mg/g, respectively. The obtained biochars are promising materials for the efficient removal of organic pollutants.

Keywords: biochar; corn cob; magnetic composite; coprecipitation; methylene blue

Citation: Guel-Nájar, N.A.; Rios-Hurtado, J.C.; Muzquiz-Ramos, E.M.; Dávila-Pulido, G.I.; González-Ibarra, A.A.; Pat-Espadas, A.M. Magnetic Biochar Obtained by Chemical Coprecipitation and Pyrolysis of Corn Cob Residues: Characterization and Methylene Blue Adsorption. *Materials* **2023**, *16*, 3127. https://doi.org/10.3390/ma16083127

Academic Editors: Wen-Tien Tsai and Carlos Javier Duran-Valle

Received: 3 March 2023
Revised: 27 March 2023
Accepted: 10 April 2023
Published: 15 April 2023

1. Introduction

Due to rapid population growth, accelerated urbanization, and industrialization, the volume and diversity of agro-industrial wastes have increased. These wastes are considered a significant source of pollution due to poor management and improper disposal [1,2] (Awogbemi and Kallon, 2022; Karić et al., 2022). A strategy to reduce the disposed residues is to prepare new materials for different applications. Biochar is a solid material obtained from the thermochemical conversion of biomass in an oxygen-limited environment [3]. It is a carbon-rich organic material that is prepared by heating biomass. Depending on the feedstock used to obtain it, the properties of the biochar such as its high specific surface area, microporosity, and ion exchange capacity can be improved [4,5]. Furthermore, corn

residues are suitable to obtain biochar due to their lignocellulosic biomass, which favors its formation [6,7].

The use of biochar as an adsorbent material has been widely studied; however, the adsorption efficiency can be improved. Surface activation or modification with chemical reagents, steam and gas, mineral oxides, organic compounds, clay minerals, and microorganisms has been widely reported [8–10]. Composite biochar is prepared by impregnating the surface with metal oxides to modify the surface properties and increase the adsorption capacity [10,11].

One of the ideal methods of surface modification is with magnetite (i.e., Fe_3O_4). This oxide is non-toxic, can improve the adsorption capacity towards various pollutants, and provides strong magnetic properties. Ion exchange, complexation, electrostatic attraction, and metal–π interaction are mechanisms that make adsorption techniques suitable. Due to its magnetic properties, Fe_3O_4 can be used to recycle biochar, as iron metal oxides allow adsorbent recovery [12–14]. This makes it important to obtain magnetic biochars for the removal of water pollutants. Santhosh et al. synthesized a magnetic biochar from sewage sludge and woodchips, for Cr (VI) removal [15]. A magnetic biochar in a single-step method was obtained for the removal of organic pollutants by Chen et al. (2022) [16]. A filamentous fungus, *Trichoderma reesei*, was used as a template for 3D biochar obtention.

Water pollution is one of the challenges facing society [17]. One of the main sources of pollutants are organic dyes such as methylene blue (MB). This dye is widely used in the textile, food, cosmetic, and pharmaceutical industries; it usually causes negative effects on photosynthetic activity [17–19]. For this reason, it is important to remove dyes using adsorbent materials, such as biochars.

To increase the MB adsorption capacity, a wide variety of precursors have been used to obtain biochars with modified surfaces. Mu et al. (2022) obtained a magnetic biochar by slow pyrolysis of tea residue powder with $FeCl_3$ solution impregnation. The authors studied MB adsorption as a dye model and described the adsorption process due to the main interactions of pore filling, hydrogen bonding, π–π interactions, and electrostatic attraction [20]. Güleç et al. (2022) prepared biochars from seaweed and rapeseed, obtaining a q_m of 117.6 and 70.9 mg/g, respectively [21]. Zeng et al. (2021) prepared a sludge-based magnetic biochar by pyrolysis and studied MB adsorption [22]. Li et al. (2022) made a biochar from moringa seed shells. In the study, Fe_3O_4 was added to activate the surface of the biochar, and a high removal of MB was observed [23].

Therefore, in this work, biochars were obtained from corn cob residues by pyrolysis. A pure biochar and a magnetite impregnated with magnetite by the coprecipitation technique prior to the pyrolysis process were obtained. Both biochars were characterized to determine their physicochemical, surface, and structural properties. MB adsorption was tested to understand the behavior of biochars when modified with Fe_3O_4.

2. Materials and Methods

2.1. Reagents

To obtain biochar, corn cob waste from the municipality of Frontera, Coahuila, was used as a precursor. The chemicals used are of reagent grade: hydrochloric acid (CTR Scientific, Monterrey, MX), ferric chloride hexahydrate ($FeCl_3 \cdot 6H_2O$), ferrous chloride tetrahydrate ($FeCl_2 \cdot 4H_2O$), and sodium hydroxide (Fermont, Monterrey, MX).

2.2. Experimental Procedures

2.2.1. Pretreatment of Samples

The corn cob waste was cut into small pieces of approximately 3 cm in length, then washed with distilled water. A part of the cleaned waste was dried at 100 °C in an ECOSHEL 9053A oven (LABOTECA, Monterrey, MX) for 24 h. The remaining corn cob was passed through the chemical coprecipitation process.

2.2.2. Chemical Coprecipitation of Magnetite in Corn Cob Waste

The coprecipitation method was based on the work of Rodriguez et al. (2019) [24]. A solution was prepared in a beaker with 50 mL of deionized water, $FeCl_3 \cdot 6H_2O$ and $FeCl_2 \cdot 4H_2O$ at a 2:1 ratio according to Equation (1):

$$2Fe^{3+} + Fe^{2+} + 8OH^- \rightarrow Fe_3O_4 + 4H_2O \quad (1)$$

The solution was heated at 50 °C for 15 min. Corn cobs cleaned of waste were placed in contact with 5 mL of Fe^{3+}:Fe^{2+} ion solution. Then, 2 mL of concentrated NaOH was added by dripping and subsequently dried at 100 °C for 24 h.

2.2.3. Obtaining Biochar from Corn Cob by Pyrolysis

The research of Lee et al. (2017) and Xie et al. (2021) was used to develop corn cob pyrolysis [25,26]. Dried corn cob residues were placed in a CARBOLITE™ CTF horizontal tube furnace (Fischer Scientific, Monterrey, MX) and heated to 500 °C for 1 h. The heating rate and N_2 flow rate were varied. The obtained sample was allowed to cool slowly at room temperature. Biochar was labeled as BCM, and the modified biochar as BCM_{Fe}.

2.2.4. Characterization of Biochar

The biochar yield was determined according to the procedure reported by Qin et al. (2020), as well as the ash content using ASTM D2866-94 (ASTM, n.d.) [27,28]. In addition, SEM and EDS analysis were performed on a HITACHI model SU8230 cold cathode SEM machine (Ciudad de México, MX) with backscattered electron and secondary electron detectors; FTIR analysis with a PerkinElmer FTIR Spectrometer Frontier (Monterrey, Mexico) in a range of 4000 to 600 cm^{-1} using 32 scans and 4 cm^{-1} resolution; XRD on a Bruker D8 ADVANCE model (Ciudad de México, MX) (CuKa: 1.54 Å, 40 mA and 40 kV); XRF analysis on a Malvern Panalytical Epsilon 1 model (Monterrey, MX); and TGA on a TA Instruments TGA 550 (Ciudad de México, MX), in a temperature range of 30 °C to 700 °C at a heating rate of 10 °C/min, using air atmosphere; and N_2 physisorption at 77 K was performed in a BEL BELSORP-miniX surface analyzer (Ciudad de México, MX).

2.2.5. Methylene Blue Adsorption Efficiency and Kinetic Models

MB adsorption efficiency was determined for both biochars. In 15 mL conical tubes, 0.02 g of biochar and 10 mL of an MB solution at different concentrations (i.e., 1, 2, 4, 8, 10, and 25 ppm) were placed in contact. The pH was adjusted to 7 ± 0.2 in an Orion StarA2110 potentiometer (Monterrey, MX). The initial concentration (C_o) absorbance of each of the solutions was measured in a Mettler Toledo UV-Vis instrument model UV5 (Ciudad de México, MX) (λ = 664 nm). Then, the tubes were placed in a LabTech LSI-3016A incubator (El Crisol, Monterrey, México) at 25 °C and 150 rpm for 24 h. Once equilibrium was reached, the remaining concentration (C_e) values were measured by UV-Vis. The maximum adsorption capacity was calculated according to Equation (2) and fitted to the Langmuir isotherm model according to Equation (3):

$$Qe = \frac{(C_O - C_e)(V)}{m} \quad (2)$$

$$q_e = \frac{q_{max} k_L C_e}{1 + k_L C_e} \quad (3)$$

where:

q_e = adsorption capacity at equilibrium, $mg \cdot g^{-1}$
C_o = initial concentration of MB solution, $mg \cdot L^{-1}$
C_e = final concentration of MB solution, $mg \cdot L^{-1}$
V = solution volume, L
m = adsorbent mass, g

q_{max} = maximum adsorption capacity, $mg \cdot g^{-1}$
k_L = adsorption energy constant, $L \cdot mg^{-1}$

For kinetic experiments, 60 mL of a 10 ppm MB solution and 60 mg of the material were placed in a beaker. Sampling was carried out during 0, 1, 3, 3, 5, 10, 20, 40, and 60 min. The concentration was measured by a UV/Vis spectrometer. The data obtained were adjusted to the pseudo-second-order model using the following equation (Equation (4)):

$$\frac{t}{q_t} = \frac{1}{k_2(q_e)^2} + \frac{1}{q_e}t \quad (4)$$

where:

t = time, min
q_t = adsorption capacity at time, $mg \cdot g^{-1}$
q_e = adsorption capacity at equilibrium, $mg \cdot g^{-1}$
k_2 = PSO constant ($g \cdot mg^{-1} \cdot g^{-1}$)

3. Results and Discussions

3.1. Biochar Yield and Ash Percentage

It is important to dry the corn cob samples prior to pyrolysis in order to calculate the amount of biochar obtained. Besides, subjecting wet feedstock samples to pyrolysis would consume energy, and carbonization would last longer [8]. In addition, a large amount of moisture in the biomass leads to the production of liquid by-products [29]. The pyrolysis experimental conditions of the BCM samples and the yield are shown in Table 1. The N_2 flow rate was tested, and for a 50 mL/min rate, the yield was 5.60%, and for a 35 L/min rate, the yield was 28.48%. Moreover, different heating ramps were tested. The results showed that when a lower heating ramp was used (5 °C/min), the biochar yield was 26.91%. However, a higher heating ramp (10 °C/min) produced a biochar yield of 28.48% and reduced the time needed to reach the pyrolysis temperature. In addition, raw and cooked corn cob (180 °C, 1 h) conditions were tested, and no significant difference in biochar yield was observed. Therefore, to obtain a higher biochar yield, an N_2 flow rate of 35 mL/min and a heating ramp of 10 °C/min were used, in which an average yield of 28.48 ± 0.098% was obtained.

Table 1. Experimental pyrolysis conditions and performance of BCM.

Sample Condition	N_2 Flow Rate (mL/min)	Heating Rate (°C/min)	Yield (%)	Average Yield (%)	Error (%)
Raw	50	10	4.90		
Raw	50	10	6.20	5.60	0.117
Raw	50	10	5.70		
Raw	35	10	25.30		
Raw	35	10	29.61	28.48	0.098
Raw	35	10	30.54		
Cooked	35	5	29.24		
Cooked	35	5	26.59	26.91	0.081
Cooked	35	5	24.91		
Cooked	35	10	22.27		
Cooked	35	10	27.43	22.45	0.218
Cooked	35	10	17.64		

In Table 2, the ash contents of different samples are shown. It can be observed that corn cob residues contain 0.4%, while BCM shows a significant increase with 4.0%, which is lower compared to what was reported by Zhao et al. (2018); these authors determined 10.79% of ash content when heating at 300 °C and 23.27% at 500 °C [30].

Table 2. Ash content of corn cob and BCM and BCM_{Fe} biochars.

Material	Ash Content (%)
Corn cob	0.4 (±0.04)
BCM	4.0 (±0.01)
BCM_{Fe}	8.0 (±0.02)

The results shown in Table 2 are also different from those reported by Mohan et al. (2014) and Xie et al. (2021), who used corn as biomass and the same carbonization temperature [26,31]. For BCM_{Fe}, an 8.0% ash content was observed, a higher amount compared to BCM, which was attributed to the presence of inorganic particles, such as iron oxides, on the surface of BCM_{Fe}, due to the melting point of iron being >1500 °C.

The biochar yield varied according to the type of biomass and the temperature used in the pyrolysis process, according to Amalina et al. (2022) [32]. Table 3 shows a comparison with biochars reported in the literature. For BCM, the results are similar to those reported by Mohan et al. (2014) [31]. However, as reported by Suo et al. (2021), an increase in the percentage can be attributed to a lower carbonization temperature [33].

Table 3. Comparison of yield and ash percentage for different biochars.

Biomass	Temperature (°C)	Yield (%)	Ash (%)	Reference
Water hyacinth	350	34.25	10.42	[34]
Corn straw	400	31.60	NR	[33]
Pigeon pea stalk	400	29.80	3.08	[35]
Corn stalk pellet	500	33.41	20.86	[26]
Corn stover	500	28.21	6.60	[31]
Sugarcane bagasse	550	21.15	1.16	[34]
Bamboo	600	27.00	4.65	[35]

Note: Not reported.

3.2. Inorganic Composition

In order to determine the ash composition, XRF analysis was performed. The results are shown in Table 4, where it can be observed the presence of elements such as K, P, and Si, which are in a higher proportion in the BCM biochar when compared with corn cobs. The amount of K increases considerably by the pyrolysis process, being the main element in BCM with a concentration greater than 11%, similar to that reported by Gómez-Vásquez et al. (2022) [36]. The high amount of elements was attributed to the fertilizer used for plant growth (Land and Water Division, FAO, 2002) since the main elemental composition is K, P, and Si with concentrations greater than 0.6% [37]. Other elements such as Cl, Fe, and S were also detected, albeit in lower concentrations. For BCM_{Fe}, an increase in Fe amount (8.761%) was attributed to the formation of iron oxides by the coprecipitation method.

Table 4. Samples composition obtained by XRF.

Element	Corn Cob		BCM		BCM_{Fe}	
	Concentration (%)	Error (%)	Concentration (%)	Error (%)	Concentration (%)	Error (%)
K	1.548	0.003	11.269	0.140	9.718	0.098
P	0.138	0.011	0.662	0.075	0.912	0.005
Si	0.786	0.033	0.604	0.309	0.478	0.361
Cl	0.174	0.003	0.555	0.414	1.236	0.047
Fe	0.529	0.002	0.208	0.027	8.761	0.152

3.3. Morphological Analysis

SEM analysis was performed to characterize the surface morphologies of the samples. Figure 1 shows the BCM surface, where a highly porous structure, a large surface area

(S_{BET}: 1013.52 m^2/g), and evenly distributed pores were observed. The pore size range was determined as mesopores and macropores, as micropores are generally more difficult to detect, according to the report by Quillope et al. (2021) [38].

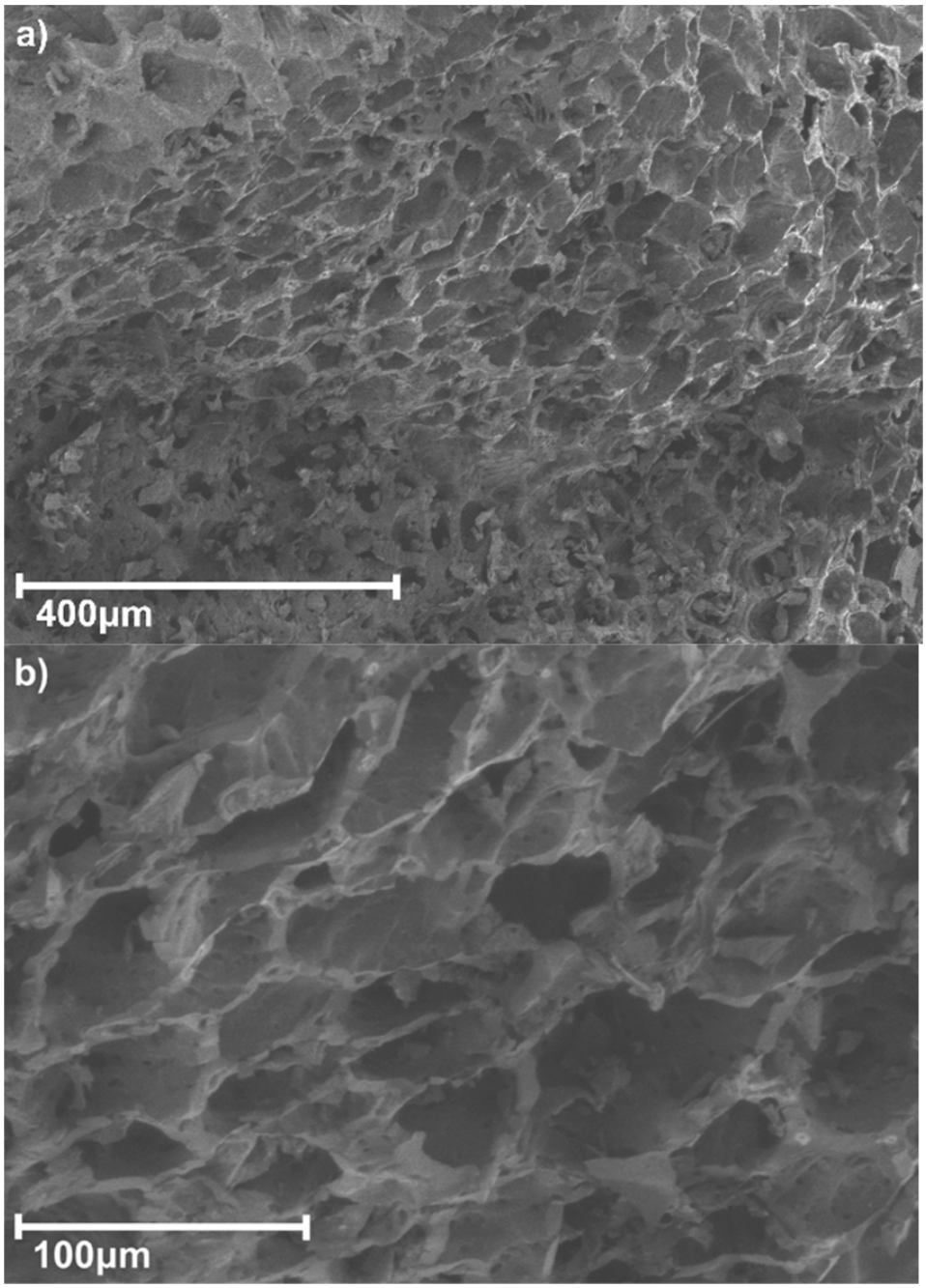

Figure 1. SEM images of the BCM structure, (**a**) 400 μm and (**b**) 100 μm.

The surface structure (S_{BET} = 903.67 m^2/g) of magnetic biochar (BCM_{Fe}) is shown in Figure 2. Particles with an intense brightness were observed, indicating the presence of an element with a higher atomic mass such as Fe [39]. Fe_3O_4 particles generally adopted a spherical shape and formed agglomerates, which were distributed over the biochar surface, according to the reports by Ouyang et al. (2017) and J. Yan et al. (2020) [40,41]. It can be determined from the SEM analysis of Figure 2 using Image-Pro Plus software that the average agglomerate diameter is 5.83 ± 2.23 μm. This is in accordance with the value

reported by Navarathna et al. (2019), in which the agglomerated particle size was up to 7 μm [42].

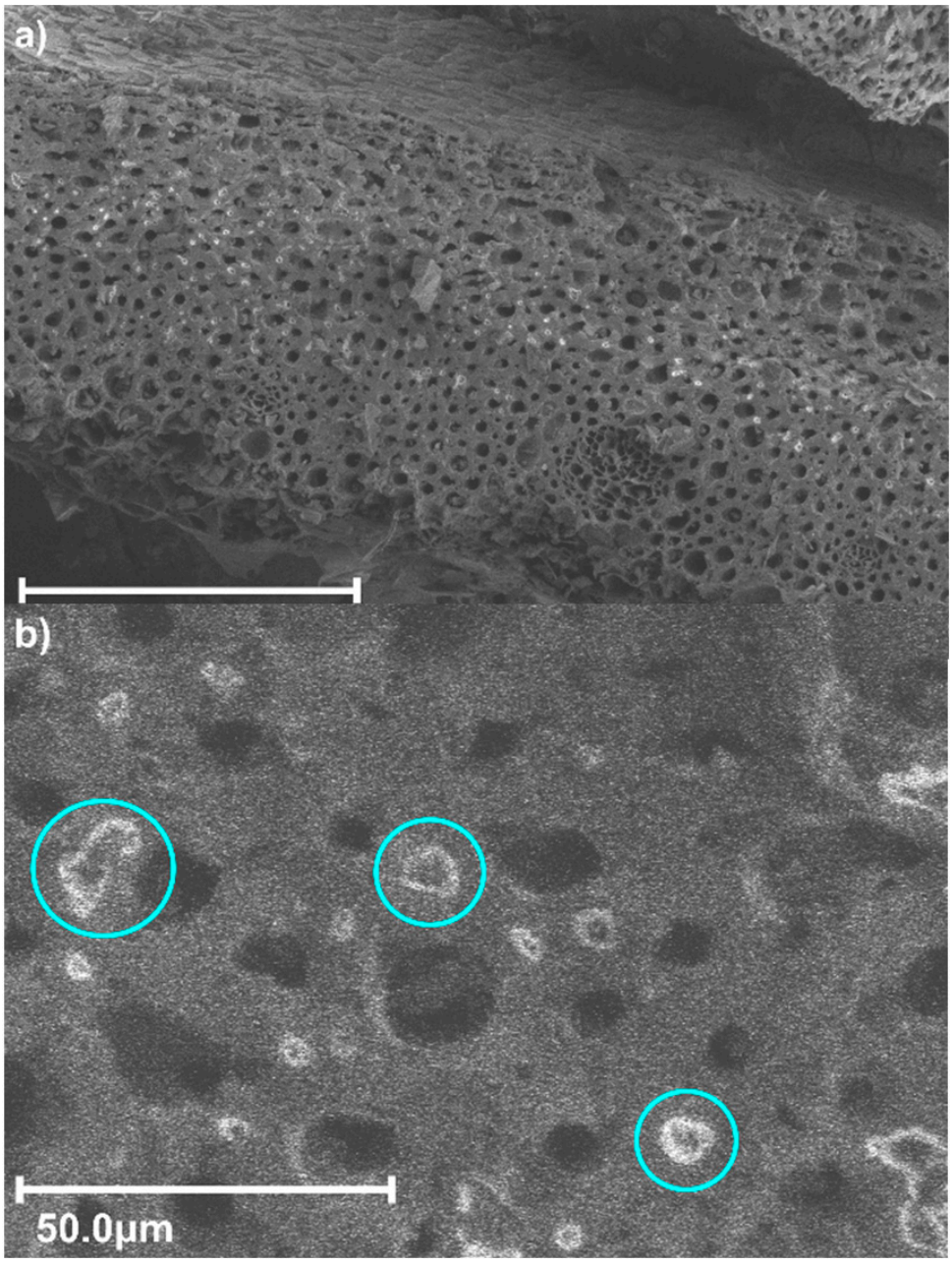

Figure 2. SEM images of the BCM_{Fe} structure, (**a**) 300 μm and (**b**) 50 μm. The blue circles represents the Fe particles observed in SEM.

The BCM_{Fe} surface elemental composition was obtained by EDS analysis. Four points of the sample (see Figure 3) were analyzed to obtain the mass percentage of each element (Table 5). Biochar BCM consists mainly of C (carbon) and O (oxygen). Other elements were also detected, although in smaller proportions. The results were consistent with those obtained by XRF analysis for Si, K, and Fe. No presence of Cl was observed in the sample, so Fe ions were transformed into iron oxide. In addition, the Fe percentage increased significantly due to the presence of Fe particles in the biochar.

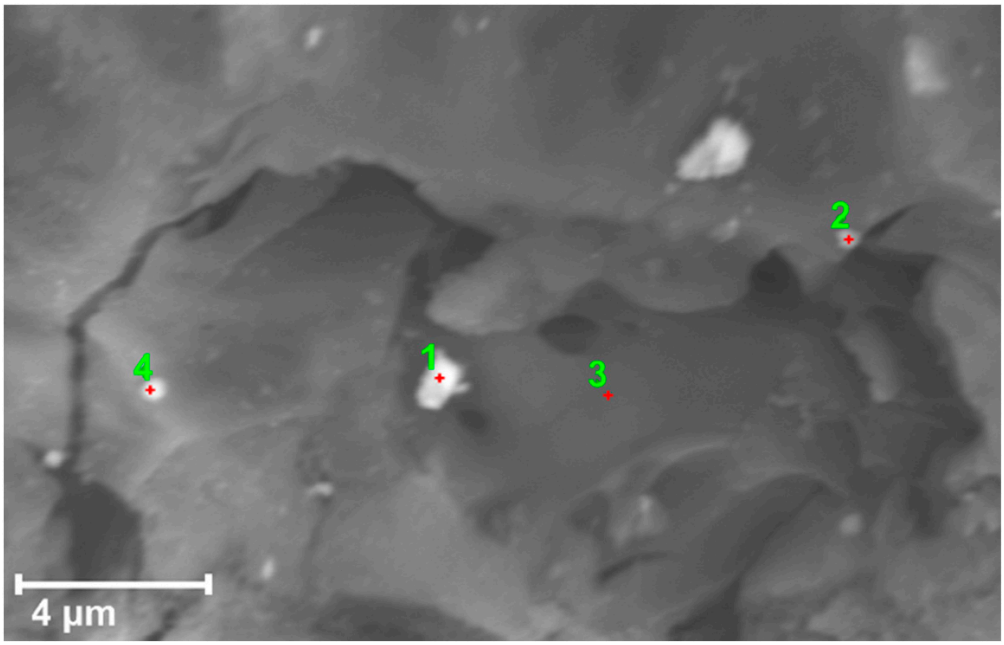

Figure 3. EDS image of the 4 BCM_{Fe} points analyzed. The numbers represents the point where EDS was done for Table 5.

Table 5. Elemental composition of BCM_{Fe}.

Element	% by Mass			
	Point 1	**Point 2**	**Point 3**	**Point 4**
C	28.84	44.33	55.91	55.78
O	8.08	27.75	22.67	31.85
Fe	46.06	7.50	3.76	4.78
Si	14.58	15.53	12.17	6.78
K	2.44	4.89	5.49	1.80
Total	100	100	100	100

3.4. Structure of Modified Biochar

The crystalline structures of the modified biochar were characterized by X-ray diffraction. The XRD pattern of the BCM_{Fe} is presented in Figure 4, which confirms that the precipitated iron ions are mainly magnetite (Fe_3O_4). A series of diffraction peaks corresponding to Fe_3O_4 were detected at 2θ values of 30.02°, 35.45°, 43.08°, 47.38°, and 62.53°, with Miller indices of (220), (311), (400), (331), and (440), respectively. The observed signals coincided with the diffraction patterns of Fe_3O_4 reported by Compeán-Jasso et al. (2008) and Peña-Rodríguez et al. (2018), confirming the successful formation of magnetite on the biochar surface [43,44].

In Figure 4, an intense signal at 29.29° due to silicon oxide (SiO_2) with crystallographic chart 96-900-0809 can be observed. Since SiO_2 is a compound that is prominent in the inorganic components of corn cob [36], or it may belong to a potassium mineral (K) with crystallographic chart 96-901-1978, these elements can be found in biochar due to the inorganic elements present in the biomass that was not carbonized. The signals for amorphous graphite were also observed at signals between 20 and 30° and 40 and 50°.

In order to identify if the material had the characteristic magnetic properties of magnetite, a simple test was carried out with the addition of a magnet to a suspension with 0.1 g of the magnetic biochar, and as can be seen in Figure 5, the material stuck to the magnet due to the magnetic properties.

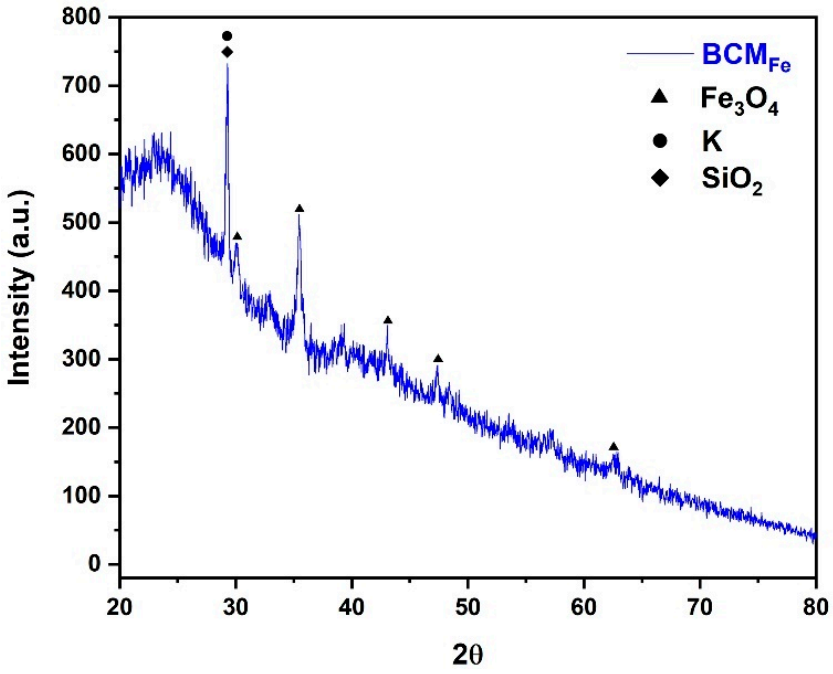

Figure 4. BCM$_{Fe}$ XRD pattern.

Figure 5. Magnetic properties of biochar (BCM$_{Fe}$).

3.5. Surface Functional Groups

An FTIR analysis was performed to observe surface functional groups on the obtained biochars. The results are presented in Figure 6, where the low intensity of the signals, which are attributed to the temperature at which the pyrolysis process was carried out, can be observed. According to Manoharan et al. (2022), the number of functional groups decreases at higher temperatures due to the release of CO_2 [45].

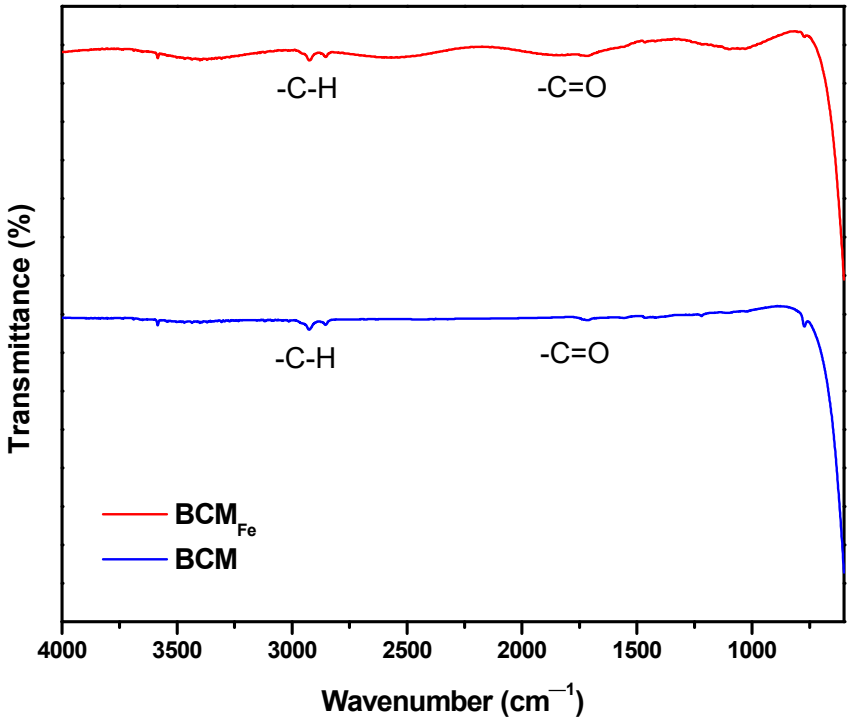

Figure 6. FTIR analysis of BCM and BCM_{Fe}.

Both biochars showed similar bands, one observed at 1712 cm^{-1}, corresponding to the C=O stretching vibration of the carbonyl group [46], which is formed during the carbonization process, and the double signals between 2800 and 3000 cm^{-1}, corresponding to -C–H aliphatic compounds stretching vibrations [35,47]. The band near 500 cm^{-1} could be described as a stretching vibration of metallic oxides due to the presence of inorganic compounds in BCM and BCM_{Fe} [48].

3.6. Thermal Behavior

Thermal analysis was carried out on both biochars (BCM and BCM_{Fe}). The thermogravimetric (TG) and differential thermogravimetric (DTG) curves of Figure 7 show two main weight loss processes for both biochars. In the first curve, BCM showed a 4% loss at 89 °C, while BCM_{Fe} showed a 10% weight loss, due to water molecules evaporating from the biochar surface. At higher temperatures, a greater reduction in weight loss was observed. In BCM, a weight loss of 93.8% was observed at 500 °C, while a weight loss of 78.6% was observed in BCM_{Fe} at 650 °C. The loss was attributed to the decomposition of lignocellulosic biomass and extracts such as proteins, fats, and sugars, among others [14,49], results observed in FTIR analysis, in addition to the loss of functional groups such as carboxyl and hydroxyl groups [50]. Compared to BCM biochar, BCM_{Fe} carbonized at a higher temperature and showed higher thermal stability, which corresponded to a greater amount of inorganic components [51].

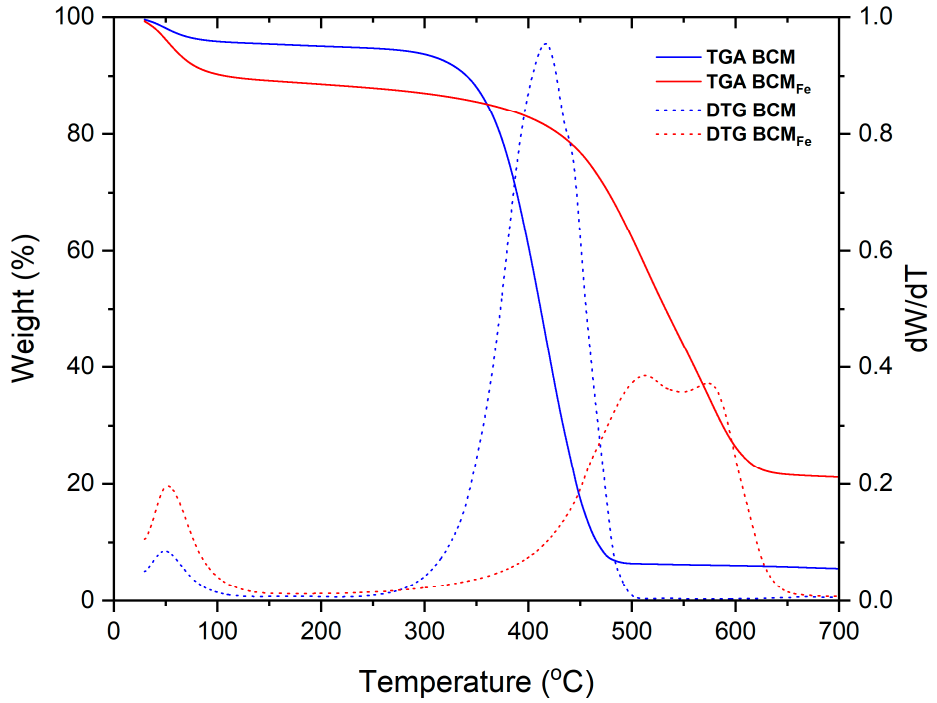

Figure 7. BCM and BCM_{Fe} biochar thermograms.

The difference between the amount of weight loss for BCM_{Fe} and BCM was 15.2% and corresponds to the F_3O_4 present on the biochar surface according to XRD results. The DTG curve of the impregnated biochar showed two signals between 400 and 650 °C, attributed to the Fe_3O_4 oxidation to α-Fe_2O_3 and γ-Fe_2O_3.

3.7. Methylene Blue Adsorption Capacity

MB adsorption capacity was studied at pH 7 since the PZC of BCM was measured as 7.06. The adsorption capacity was adjusted to the Langmuir model, as can be seen in Figure 8. Non-linear regression was used to adjust the experimental data using Origin® software. BCM biochar showed a maximum adsorption capacity (q_m) of 23.17 mg/g and BCM_{Fe} biochar of 39.66 mg/g, as shown in Table 6.

The q_m of BCM_{Fe} biochar is similar to that reported by Zeng et al. (2021), with a q_m of 39.35 mg/g at a temperature of 35 °C, using a sewage sludge-based magnetic biochar (Fe_3O_4) by pyrolysis for the removal of methylene blue in water [22]. Mubarak et al. (2015) prepared a magnetic biochar derived from an empty fruit bunch treated with ferric chloride ($FeCl_3$) to remove methylene blue, obtaining a q_m of 31.25 mg/g [52], while Ruthiraan et al. (2017) obtained a qm of 46.30 mg/g in MB removal with a magnetic iron oxide biochar (impregnated with Fe_2O_3 solution) obtained from mangosteen peel [53].

In addition to q_m, Table 6 shows the k_L, R_L, and R^2 parameters. The Langmuir constant (k_L) indicates the degree of interaction between the adsorbate and the surface. When the adsorption energy constant (k_L) was less than 1, it indicates that there was a strong interaction between the adsorbate and the adsorbent. The Langmuir separation factor (R_L) showed values lower than 1 in both biochars, which indicated an appropriate adsorption process. If $R_L > 1$ is not suitable, while if $0 < R_L < 1$ is appropriate [54].

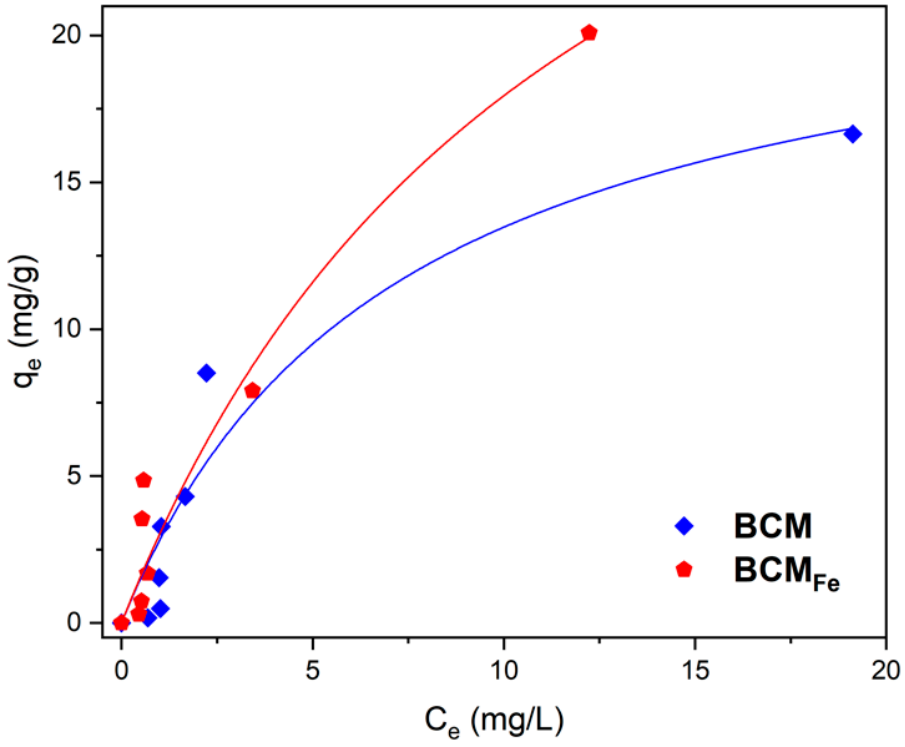

Figure 8. Methylene blue adsorption isotherm adjusted to the Langmuir model for the synthesized samples. pH = 7; T = 25 °C; dosage = 0.02 g/10 mL; methylene blue C_o = 1–25 ppm.

Table 6. Langmuir model parameters.

Material	q_m (mg/g)	k_L (L/mg)	R_L	R^2 (%)
BCM	23.17	0.14	0.22–0.88	99.44%
BCM_{Fe}	39.66	0.08	0.33–0.92	99.61%

Further, the linear correlation coefficient (R^2) was high, so the adsorption isotherms fit well for the Langmuir model. This model indicates that the adsorbent surface was completely flat and homogeneous and that each surface site can only hold one molecule of the adsorbate, resulting in monolayer-type adsorption [55,56]. The metal–π interaction is one of the mechanisms reported in the literature for organic compounds in modified biochars with metallic oxides [57–60]. By this, an increase in the MB adsorption capacity for BCM_{Fe} was observed, due to the presence of Fe_3O_4 particles on the surface. Several reports have corroborated that MB adsorption by activated carbons from lignocellulosic materials demonstrates a strong correlation with the Langmuir isotherm equation [61].

Furthermore, experimental data were adjusted to the PFO and PSO order kinetic models; however, both biochars were better fitted to the PSO ($R^2 > 0.998$) (Figure 9). The PSO model describes the adsorption process in a surface monolayer. The results agreed with those observed in adsorption isotherms.

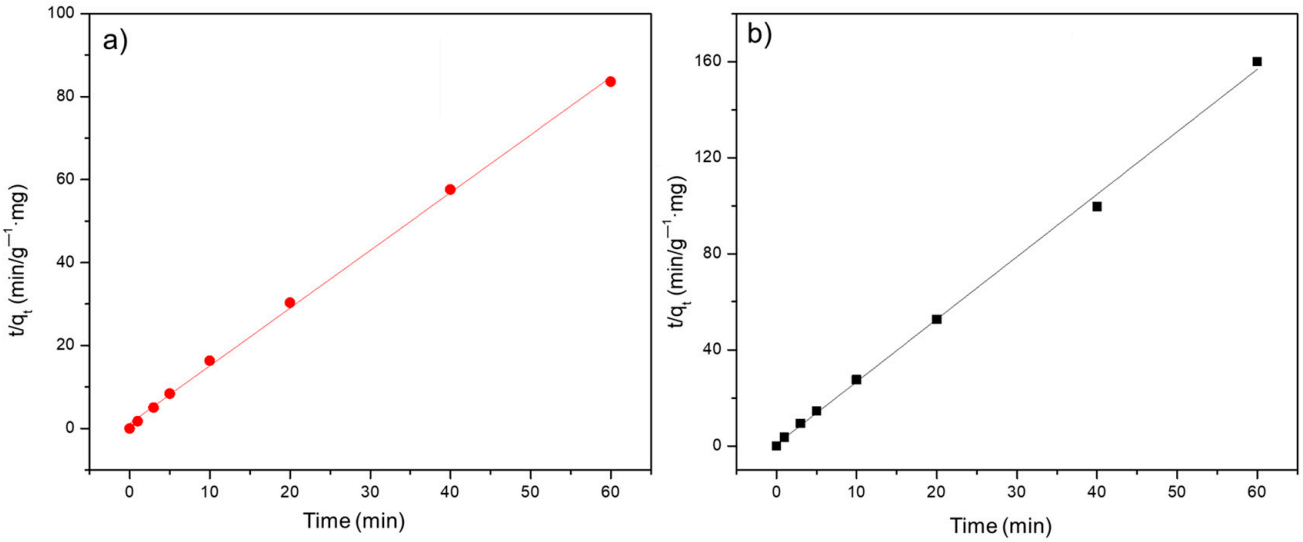

Figure 9. Kinetic PSO model adjust for BCM (**a**) and BCM_{Fe} (**b**).

4. Conclusions

The results showed that the yield of BCM was 28.483%, higher than that of BCM_{Fe} (i.e., 26.160%). Both biochars show a highly porous surface, a large surface area, and uniformly distributed pores and they are mainly composed of C and O, in addition to Fe, Si, and K. BCM_{Fe} biochar contains a higher amount of Fe compared to BCM due to its impregnation with Fe ions, successfully achieving the addition of Fe_3O_4 particles, and XRD analysis supports this result.

While the ash content of BCM was 4% lower than BCM_{Fe} (i.e., 8%), there were 4% more inorganic compounds in BCM_{Fe}. Both biochars presented carbonyl and aliphatic groups on the surface. The TGA revealed that BCM carbonizes at 500 °C with a weight loss of 93.8%, while BCMFe carbonizes at 650 °C with a weight loss of 78.6%. The above indicates that BCM_{Fe} showed higher thermal stability.

It was possible to obtain a material capable of removing the organic pollutant methylene blue, with a maximum adsorption capacity of 23.17 mg/g and 39.66 mg/g for BCM and BCM_{Fe} biochar, respectively. The modified biochar (BCM_{Fe}) showed a higher adsorption capacity (i.e., 71.17%) than BCM.

Author Contributions: N.A.G.-N. performed the experimental part, wrote the introduction and methods of the manuscript; J.C.R.-H. designed the experimentation, followed up on the methodology and supervised the discussion of the manuscript; E.M.M.-R. supported in the thermodynamic experiments of methylene blue adsorption and analyzed the results; G.I.D.-P. supported in experimentation and discussion of characterizations; A.A.G.-I. supported in the discussion of the results and language revision; A.M.P.-E. supported in the materials characterization. All authors have read and agreed to the published version of the manuscript.

Funding: Norma Araceli Guel-Nájar received a grant from CONACyT. Grant number 620952; Jorge Carlos Rios-Hurtado received a financial support for the project from COECyT. Project number FONCyT COAH-2021-C15-C013.

Institutional Review Board Statement: Not applicable.

Informed Consent Statement: Not applicable.

Data Availability Statement: Not applicable.

Acknowledgments: The grant (620952) awarded by the Consejo Nacional de Ciencia y Tecnología (CONACYT) is gratefully acknowledged for Guel-Najar, and all authors thank the Fondo de Investigación Científica y Tecnológica (FONCyT COAH-2021-C15-C013) for the financial support of this project.

Conflicts of Interest: We know of no conflicts of interest associated with this publication, and there has been no significant financial support for this work that could have influenced its outcome.

References

1. Awogbemi, O.; Von Kallon, D.V. Pretreatment techniques for agricultural waste. *Case Stud. Chem. Environ. Eng.* **2022**, *6*, 100229. [CrossRef]
2. Karić, N.; Maia, A.S.; Teodorović, A.; Atanasova, N.; Langergraber, G.; Crini, G.; Ribeiro, A.R.L.; Đolić, M. Bio-waste valorisation: Agricultural wastes as biosorbents for removal of (in)organic pollutants in wastewater treatment. *Chem. Eng. J. Adv.* **2022**, *9*, 100239. [CrossRef]
3. International Biochar Initiative. Standardized Product Definition and Product Testing Guidelines for Biochar That Is Used in Soil. International Biochar Initiative, November, 1–61. 2015. Available online: https://www.biochar-international.org/wp-content/uploads/2018/04/IBI_Biochar_Standards_V2.1_Final.pdf (accessed on 13 January 2023).
4. Mehdi, R.; Khoja, A.H.; Naqvi, S.R.; Gao, N.; Amin, N.A.S. A Review on Production and Surface Modifications of Biochar Materials via Biomass Pyrolysis Process for Supercapacitor Applications. *Catalysts* **2022**, *12*, 798. [CrossRef]
5. Saravanan, A.; Senthil Kumar, P. Biochar derived carbonaceous material for various environmental applications: Systematic review. *Environ. Res.* **2022**, *214*, 113857. [CrossRef] [PubMed]
6. Tehreem, S.; Yousra, M.; Alamer, K.H.; Alsudays, I.M.; Sarwar, S.; Kamal, A.; Naeem, S. Analysis of the role of various biochar in the remediation of heavy metals in contaminated water and its kinetics study. *J. Saudi Chem. Soc.* **2022**, *26*, 101518. [CrossRef]
7. Wang, L.; Olsen, M.N.P.; Moni, C.; Dieguez-Alonso, A.; de la Rosa, J.M.; Stenrød, M.; Liu, X.; Mao, L. Comparison of properties of biochar produced from different types of lignocellulosic biomass by slow pyrolysis at 600 °C. *Appl. Energy Combust. Sci.* **2022**, *12*, 100090. [CrossRef]
8. Amalina, F.; Syukor Abd Razak, A.; Krishnan, S.; Sulaiman, H.; Zularisam, A.W.; Nasrullah, M. Advanced techniques in the production of biochar from lignocellulosic biomass and environmental applications. *Clean. Mater.* **2022**, *6*, 100137. [CrossRef]
9. Li, R.; Wu, Y.; Lou, X.; Li, H.; Cheng, J.; Shen, B.; Qin, L. Porous Biochar Materials for Sustainable Water Treatment: Synthesis, Modification, and Application. *Water* **2023**, *15*, 395. [CrossRef]
10. Huang, W.H.; Lee, D.J.; Huang, C. Modification on biochars for applications: A research update. *Bioresour. Technol.* **2021**, *319*, 124100. [CrossRef]
11. Roy, H.; Islam, M.S.; Arifin, M.T.; Firoz, S.H. Synthesis, Characterization and Sorption Properties of Biochar, Chitosan and ZnO-Based Binary Composites towards a Cationic Dye. *Sustainability* **2022**, *14*, 14571. [CrossRef]
12. Isaac, R.; Siddiqui, S. Sequestration of Ni(II) and Cu(II) using FeSO4 modified Zea mays husk magnetic biochar: Isotherm, kinetics, thermodynamic studies and RSM. *J. Hazard. Mater. Adv.* **2022**, *8*, 100162. [CrossRef]
13. Pipíška, M.; Krajcíková, E.K.; Hvostik, M.; Frišták, V.; Duriška, L.; Cernicková, I.; Kanuchová, M.; Conte, P.; Soja, G. Biochar from Wood Chips and Corn Cobs for Adsorption of Thioflavin T and Erythrosine B. *Materials* **2022**, *15*, 1492. [CrossRef] [PubMed]
14. Xu, Z.; Hu, Y.; Guo, Z.; Xiao, X.; Peng, C.; Zeng, P. Optimizing pyrolysis temperature of contaminated rice straw biochar: Heavy metal(loid) deportment, properties evolution, and Pb adsorption/immobilization. *J. Saudi Chem. Soc.* **2022**, *26*, 101439. [CrossRef]
15. Santhosh, C.; Daneshvar, E.; Tripathi, K.M.; Baltrėnas, P.; Kim, T.; Baltrėnaitė, E.; Bhatnagar, A. Synthesis and characterization of magnetic biochar adsorbents for the removal of Cr(VI) and Acid orange 7 dye from aqueous solution. *Environ. Sci. Pollut. Res.* **2020**, *27*, 32874–32887. [CrossRef] [PubMed]
16. Chen, X.; Lin, J.; Su, Y.; Tang, S. One-Step Carbonization Synthesis of Magnetic Biochar with 3D Network Structure and Its Application in Organic Pollutant Control. *Int. J. Mol. Sci.* **2022**, *23*, 12579. [CrossRef] [PubMed]
17. Ghanbari, N.; Ghafuri, H. Design and preparation the novel polymeric layered double hydroxide nanocomposite (LDH/Polymer) as an efficient and recyclable adsorbent for the removal of methylene blue dye from water. *Environ. Technol. Innov.* **2022**, *26*, 102377. [CrossRef]
18. Oladoye, P.O.; Ajiboye, T.O.; Omotola, E.O.; Oyewola, O.J. Methylene blue dye: Toxicity and potential technologies for elimination from (waste)water. *Results Eng.* **2022**, *16*, 100678. [CrossRef]
19. Ramutshatsha-Makhwedzha, D.; Mavhungu, A.; Moropeng, M.L.; Mbaya, R. Activated carbon derived from waste orange and lemon peels for the adsorption of methyl orange and methylene blue dyes from wastewater. *Heliyon* **2022**, *8*, e09930. [CrossRef]
20. Mu, Y.; Du, H.; He, W.; Ma, H. Functionalized mesoporous magnetic biochar for methylene blue removal: Performance assessment and mechanism exploration. *Diamond Rel. Mat.* **2022**, *121*, 108795. [CrossRef]
21. Güleç, F.; Williams, O.; Kostas, E.T.; Samson, A.; Stevens, L.A.; Lester, E. A comprehensive comparative study on methylene blue removal from aqueous solution using biochars produced from rapeseed, whitewood, and seaweed via different thermal conversion technologies. *Fuel* **2022**, *330*, 125428. [CrossRef]
22. Zeng, H.; Qi, W.; Zhai, L.; Wang, F.; Zhang, J.; Li, D. Preparation and characterization of sludge-based magnetic biochar by pyrolysis for methylene blue removal. *Nanomaterials* **2021**, *11*, 2473. [CrossRef] [PubMed]

23. Li, M.; Dong, C.; Guo, C.; Yu, L. Magnetic Activated Biochar Fe_3O_4-MOS Made from Moringa Seed Shells for the Adsorption of Methylene Blue. *Processes* **2022**, *10*, 2720. [CrossRef]
24. Rodríguez, J.A.; Ríos, J.C.; Flores, S.F.; Treviño, G.G.; Muzquiz, E.M. Síntesis y caracterización de compositos carbón/óxidos de hierro a partir de caña de azúcar. *Theorema* **2019**, *10*, 124–129.
25. Lee, X.J.; Lee, L.Y.; Gan, S.; Thangalazhy-Gopakumar, S.; Ng, H.K. Biochar potential evaluation of palm oil wastes through slow pyrolysis: Thermochemical characterization and pyrolytic kinetic studies. *Bioresour. Technol.* **2017**, *236*, 155–163. [CrossRef]
26. Xie, R.; Zhu, Y.; Zhang, H.; Zhang, P.; Han, L. Effects and mechanism of pyrolysis temperature on physicochemical properties of corn stalk pellet biochar based on combined characterization approach of microcomputed tomography and chemical analysis. *Bioresour. Technol.* **2021**, *329*, 124907. [CrossRef]
27. Qin, L.; Wu, Y.; Hou, Z.; Jiang, E. Influence of biomass components, temperature and pressure on the pyrolysis behavior and biochar properties of pine nut shells. *Bioresour. Technol.* **2020**, *313*, 123682. [CrossRef] [PubMed]
28. ASTM. Método de Prueba Estándar Para Contenido Total de Cenizas de Carbón Activado. Available online: https://www.astm.org/d2866-94r04.html (accessed on 8 November 2022).
29. Al-Rumaihi, A.; Shahbaz, M.; Mckay, G.; Mackey, H.; Al-Ansari, T. A review of pyrolysis technologies and feedstock: A blending approach for plastic and biomass towards optimum biochar yield. *Renew. Sustain. Energy Rev.* **2022**, *167*, 112715. [CrossRef]
30. Zhao, N.; Yin, Z.; Liu, F.; Zhang, M.; Lv, Y.; Hao, Z.; Pan, G.; Zhang, J. Environmentally persistent free radicals mediated removal of Cr(VI) from highly saline water by corn straw biochars. *Bioresour. Technol.* **2018**, *260*, 294–301. [CrossRef]
31. Mohan, D.; Kumar, S.; Srivastava, A. Fluoride removal from ground water using magnetic and nonmagnetic corn stover biochars. *Ecol. Eng.* **2014**, *73*, 798–808. [CrossRef]
32. Amalina, F.; Razak, A.S.A.; Krishnan, S.; Zularisam, A.W.; Nasrullah, M. A comprehensive assessment of the method for producing biochar, its characterization, stability, and potential applications in regenerative economic sustainability—A review. *Clean. Mater.* **2022**, *3*, 100045. [CrossRef]
33. Suo, F.; You, X.; Yin, S.; Wu, H.; Zhang, C.; Yu, X.; Sun, R.; Li, Y. Preparation and characterization of biochar derived from co-pyrolysis of Enteromorpha prolifera and corn straw and its potential as a soil amendment. *Sci. Total Environ.* **2021**, *798*, 149167. [CrossRef] [PubMed]
34. Muigai, H.H.; Bordoloi, U.; Hussain, R.; Ravi, K.; Moholkar, V.S.; Kalita, P. A comparative study on synthesis and characterization of biochars derived from lignocellulosic biomass for their candidacy in agronomy and energy applications. *Int. J. Energy Res.* **2021**, *45*, 4765–4781. [CrossRef]
35. Sahoo, S.S.; Vijay, V.K.; Chandra, R.; Kumar, H. Production and characterization of biochar produced from slow pyrolysis of pigeon pea stalk and bamboo. *Clean. Eng. Technol.* **2021**, *3*, 100101. [CrossRef]
36. Gómez-Vásquez, R.; Fernández-Ballesteros, E.; Camargo-Trillos, D. Biogenic nanoporous oxides recovery from by-products of bioenergy production: Rice husks and corncob biochars. *Biomass Bioenergy* **2022**, *161*, 106455. [CrossRef]
37. Land and Water Division-FAO. Fertilizantes, su presentación, calidad y etiquetado. In *Los Fertilizantes y Su Uso*; IFA: Paris, France, 2002; pp. 33–44.
38. Quillope, J.C.C.; Carpio, R.B.; Gatdula, K.M.; Detras, M.C.M.; Doliente, S.S. Optimization of process parameters of self-purging microwave pyrolysis of corn cob for biochar production. *Heliyon* **2021**, *7*, e08417. [CrossRef] [PubMed]
39. Leichtweis, J.; Silvestri, S.; Carissimi, E. New composite of pecan nutshells biochar-ZnO for sequential removal of acid red 97 by adsorption and photocatalysis. *Biomass Bioenergy* **2020**, *140*, 105648. [CrossRef]
40. Ouyang, D.; Yan, J.; Qian, L.; Chen, Y.; Han, L.; Su, A.; Zhang, W.; Ni, H.; Chen, M. Degradation of 1,4-dioxane by biochar supported nano magnetite particles activating persulfate. *Chemosphere* **2017**, *184*, 609–617. [CrossRef]
41. Yan, J.; Yang, L.; Qian, L.; Han, L.; Chen, M. Nano-magnetite supported by biochar pyrolyzed at different temperatures as hydrogen peroxide activator: Synthesis mechanism and the effects on ethylbenzene removal. *Environ. Pollut.* **2020**, *261*, 114020. [CrossRef]
42. Navarathna, C.M.; Karunanayake, A.G.; Gunatilake, S.R.; Pittman, C.U.; Perez, F.; Mohan, D.; Mlsna, T. Removal of Arsenic(III) from water using magnetite precipitated onto Douglas fir biochar. *J. Environ. Manag.* **2019**, *250*, 109429. [CrossRef]
43. Compeán-Jasso, M.E.; Ruiz, F.; Martínez, J.R.; Herrera-Gómez, A. Magnetic properties of magnetite nanoparticles synthesized by forced hydrolysis. *Mater. Lett.* **2008**, *62*, 4248–4250. [CrossRef]
44. Peña-Rodríguez, G.; Rivera-Suárez, P.A.; González-Gómez, C.H.; Parra-Vargas, C.A.; Garzón-Posada, A.O.; Landínez-Téllez, D.A.; Roa-Rojas, J. Efecto de la concentración de magnetita en la estructura, propiedades eléctricas y magnéticas de un material compuesto a base de resina de poliéster. *TecnoLógicas* **2018**, *21*, 13–27. [CrossRef]
45. Manoharan, T.; Ganeshalingam, S.; Nadarajah, K. Mechanisms of emerging contaminants removal by novel neem chip biochar. *Environ. Adv.* **2022**, *7*, 100158. [CrossRef]
46. Binh, Q.A.; Nguyen, H.H. Investigation the isotherm and kinetics of adsorption mechanism of herbicide 2,4-dichlorophenoxyacetic acid (2,4-D) on corn cob biochar. *Bioresour. Technol. Rep.* **2020**, *11*, 100520. [CrossRef]
47. Bekiaris, G.; Peltre, C.; Jensen, L.S.; Bruun, S. Using FTIR-photoacoustic spectroscopy for phosphorus speciation analysis of biochars. *Spectrochim. Acta Part A Mol. Biomol. Spectrosc.* **2016**, *168*, 29–36. [CrossRef] [PubMed]
48. Ríos Hurtado, J.C.; Martínez-Valdés, A.C.; Rangel Méndez, J.R.; Ballesteros Pacheco, J.C.; Múzquiz Ramos, E.M. Facile synthesis and characterization of $MnxZn_{1-x}Fe_2O_4$/activated carbon composites for biomedical applications. *J. Ceram. Sci. Technol.* **2016**, *7*, 289–294. [CrossRef]

49. Parthasarathy, P.; Fernandez, A.; Singh, D.K.; Al-Ansari, T.; Mackey, H.R.; Rodriguez, R.; Mazza, G.; Tirkey, J.V.; McKay, G. Thermogravimetric analysis of camel dung, date stone, and their blend for pyrolytic, kinetic, and thermodynamic studies. *Clean. Chem. Eng.* **2022**, *4*, 100072. [CrossRef]
50. Lu, J.; Yang, Y.; Liu, P.; Li, Y.; Huang, F.; Zeng, L.; Liang, Y.; Li, S.; Hou, B. Iron-montmorillonite treated corn straw biochar: Interfacial chemical behavior and stability. *Sci. Total Environ.* **2020**, *708*, 134773. [CrossRef]
51. Neeli, S.T.; Ramsurn, H. Synthesis and formation mechanism of iron nanoparticles in graphitized carbon matrices using biochar from biomass model compounds as a support. *Carbon* **2018**, *134*, 480–490. [CrossRef]
52. Mubarak, N.M.; Fo, Y.T.; Al-Salim, H.S.; Sahu, J.N.; Abdullah, E.C.; Nizamuddin, S.; Jayakumar, N.S.; Ganesan, P. Removal of Methylene Blue and Orange-G from Waste Water Using Magnetic Biochar. *Int. J. Nanosci.* **2015**, *14*, 1550009. [CrossRef]
53. Ruthiraan, M.; Abdullah, E.C.; Mubarak, N.M.; Noraini, M.N. A promising route of magnetic based materials for removal of cadmium and methylene blue from waste water. *J. Environ. Chem. Eng.* **2017**, *5*, 1447–1455. [CrossRef]
54. Baytar, O.; Abdullah Ceyhan, A.; Şahin, O. Production of activated carbon from Elaeagnus angustifolia seeds using H_3PO_4 activator and methylene blue and malachite green adsorption. *Int. J. Phytoremed.* **2021**, *23*, 693–703. [CrossRef] [PubMed]
55. Hanaor, D.A.H.; Ghadiri, M.; Chrzanowski, W.; Gan, Y. Scalable surface area characterization by electrokinetic analysis of complex anion adsorption. *Langmuir* **2014**, *30*, 15143–15152. [CrossRef] [PubMed]
56. Van Hoa, N.; Minh, N.C.; Cuong, H.N.; Dat, P.A.; Nam, P.V.; Viet, P.H.T.; Phuong, P.T.D.; Trung, T.S. Highly Porous Hydroxyapatite/Graphene Oxide/Chitosan Beads as an Efficient Adsorbent for Dyes and Heavy Metal Ions Removal. *Molecules* **2021**, *26*, 6127. [CrossRef]
57. Lee, X.J.; Lee, L.Y.; Hiew, B.Y.Z.; Gan, S.; Thangalazhy-Gopakumar, S.; Ng, H.K. Valorisation of oil palm wastes into high yield and energy content biochars via slow pyrolysis: Multivariate process optimisation and combustion kinetic studies. *Mater. Sci. Energy Technol.* **2020**, *3*, 601–610. [CrossRef]
58. Li, Y.; Zhang, Y.; Zhang, Y.; Wang, G.; Li, S.; Han, R.; Wei, W. Reed biochar supported hydroxyapatite nanocomposite: Characterization and reactivity for methylene blue removal from aqueous media. *J. Mol. Liq.* **2018**, *263*, 53–63. [CrossRef]
59. Sun, L.; Wan, S.; Luo, W. Biochars prepared from anaerobic digestion residue, palm bark, and eucalyptus for adsorption of cationic methylene blue dye: Characterization, equilibrium, and kinetic studies. *Bioresour. Technol.* **2013**, *140*, 406–413. [CrossRef]
60. Wang, J.; Wang, S. Preparation, modification and environmental application of biochar: A review. *J. Clean. Prod.* **2019**, *227*, 1002–1022. [CrossRef]
61. Patawat, C.; Silakate, K.; Chuan-Udom, S.; Supanchaiyamat, N.; Hunt, A.J.; Ngernyen, Y. Preparation of activated carbon from *Dipterocarpus alatus* fruit and its application for methylene blue adsorption. *RSC Adv.* **2020**, *10*, 21082–21091. [CrossRef]